Received: 29 June 2023 | Revised: 19 October 2023 | Accepted: 29 November 2023

DOI: 10.4218/etrij.2023-0250

ORIGINAL ARTICLE

ETRI Journal WILEY

Effects of parasitic gate capacitance and gate resistance on radiofrequency performance in $L_G = 0.15$ μm GaN high-electron-mobility transistors for X-band applications

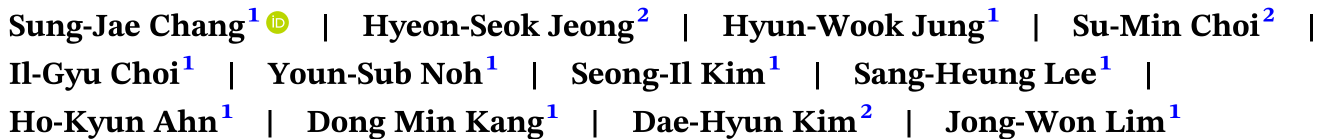

Sung-Jae Chang[1] | Hyeon-Seok Jeong[2] | Hyun-Wook Jung[1] | Su-Min Choi[2] | Il-Gyu Choi[1] | Youn-Sub Noh[1] | Seong-Il Kim[1] | Sang-Heung Lee[1] | Ho-Kyun Ahn[1] | Dong Min Kang[1] | Dae-Hyun Kim[2] | Jong-Won Lim[1]

[1]Terrestrial & Non-Terrestrial Integrated Telecommunications Research Laboratory, Electronics and Telecommunications Research Institute, Daejeon, Republic of Korea

[2]Department of Electronics and Electrical Engineering, Kyungpook National University, Daejeon, Republic of Korea

Correspondence
Sung-Jae Chang, Terrestrial & Non-Terrestrial Integrated Telecommunications Research Laboratory, Electronics and Telecommunications Research Institute, Daejeon, Republic of Korea.
Email: sjchang@etri.re.kr

Funding information
This research was supported by the National Research Foundation of Korea (NRF) grant funded by the Korea government (MIST) (No. NRF-2021M3C1C3097672).

Abstract

The effects of the parasitic gate capacitance and gate resistance (R_g) on the radiofrequency (RF) performance are investigated in $L_G = 0.15$ μm GaN high-electron-mobility transistors with T-gate head size ranging from 0.83 to 1.08 μm. When the device characteristics are compared, the difference in DC characteristics is negligible. The RF performance in terms of the current-gain cut-off frequency (f_T) and maximum oscillation frequency (f_{max}) substantially depend on the T-gate head size. For clarifying the T-gate head size dependence, small-signal modeling is conducted to extract the parasitic gate capacitance and R_g. When the T-gate head size is reduced from 1.08 to 0.83 μm, R_g increases by 82%, while f_T and f_{max} improve by 27% and 26%, respectively, because the parasitic gate–source and gate–drain capacitances reduce by 19% and 43%, respectively. Therefore, minimizing the parasitic gate capacitance is more effective that reducing R_g in our transistor design and fabrication, leading to improved RF performance when reducing the T-gate head size.

KEYWORDS
GaN, gate head size, gate resistance, high-electron-mobility transistor, parasitic gate capacitance, small-signal modeling, T-gate

1 | INTRODUCTION

The communication (transmission and reception) module is a common electronic component in terrestrial wireless communication, satellite communication, and radar systems. Among the available electronic technologies, semiconductor technologies, which are employed for data transmission and reception, are key in a communication module. The semiconductors used for building a communication module should operate in the millimeter-wave or submillimeter-wave band [1].

High-electron-mobility transistors (HEMTs) are widely used in modern communication modules owing to their low noise, high gain, and excellent radiofrequency (RF) performance [2–5]. Recently, GaN HEMTs for communication modules have been

This is an Open Access article distributed under the term of Korea Open Government License (KOGL) Type 4: Source Indication + Commercial Use Prohibition + Change Prohibition (http://www.kogl.or.kr/info/licenseTypeEn.do).
1225-6463/$ © 2024 ETRI

intensively studied. Compared with other technologies such as InP and GaAs HEMTs, GaN HEMTs provide a higher output power because GaN exhibits a high breakdown electric field, high carrier density, high mobility at the heterointerface, and wide bandgap [6–8]. However, the RF performance of GaN HEMTs in terms of the current-gain cut-off frequency (f_T) and maximum oscillation frequency (f_{max}) is lower than that of other types of HEMTs. To overcome this issue and improve the RF performance, various approaches have been proposed, such as the T-gate structure [9–12], surface passivation [13–15], n^+-regrown source–drain contact [16, 17], thin-barrier epitaxial structures [18–20], and graded channels [21, 22].

f_T and f_{max} are common indicators of the performance of RF devices including HEMTs. In GaN HEMTs, f_T and f_{max} are determined by various components of the small-signal equivalent circuit as follows [23, 24]:

$$f_T = \frac{g_m}{2\pi(C_{gs}+C_{gd})[1+(R_s+R_d)g_{ds}]+C_{gd}g_m(R_s+R_d)}, \tag{1}$$

$$f_{max} = \frac{f_T}{2\sqrt{((R_g+R_s+R_{gs})g_{ds}+2\pi f_T C_{gd} R_g)}}, \tag{2}$$

where g_m is the transconductance and the other parameters are depicted in the small-signal equivalent circuit in Figure 1.

Although the effects of other components cannot be neglected, the parasitic gate capacitances involving the parasitic gate–source (C_{gs}) and gate–drain (C_{gd}) capacitances as well as the gate resistance (R_g) substantially affect the RF performance of GaN HEMTs [24]. Therefore, to improve the RF performance, the parasitic gate capacitance and gate resistance should be minimized.

Among the approaches employed for frequency performance improvement [9–22], the T-gate structure [9–12] has been extensively applied to reduce the gate resistance (R_g). However, the parasitic gate capacitance is incompatible with R_g. When the gate head of the T-gate electrode is enlarged, R_g reduces. However, the parasitic gate capacitance increases because of the increased area under the T-gate head, as illustrated in Figure 2. Therefore, the impact of the parasitic gate capacitance and R_g on the RF performance should be thoroughly evaluated.

In this study, we experimentally investigated and compared the effects of the parasitic gate capacitance and gate resistance R_g on the RF performance of GaN HEMTs. We processed 0.15 μm-gate GaN HEMTs for different T-gate head sizes because the 0.15 μm length is currently used in X-band applications of GaN HEMTs. When the T-gate head size decreased from 1.08 μm to 0.83 μm, no notable difference was observed in the DC characteristics. Unlike earlier reports [9–12], with decreasing T-gate head size, we found that f_T and f_{max} (i.e., the RF performance) improved by 27% and 26%, respectively, despite R_g increasing by 82%. By contrast, C_{gs} and C_{gd} reduced by 19% and 43%, respectively, when the T-gate head size was reduced. Therefore, the reduction in the parasitic gate capacitance is more relevant than the reduction in R_g for improving the RF performance in GaN HEMT design and fabrication.

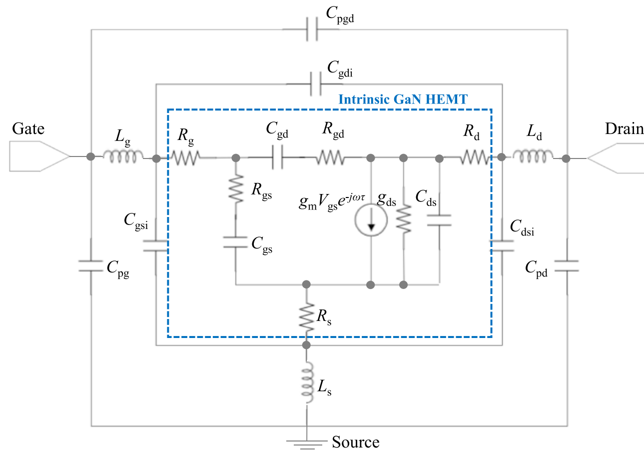

FIGURE 1 Small-signal equivalent circuit model of GaN HEMT.

2 | DEVICE FABRICATION AND MEASUREMENTS

We fabricated GaN HEMTs with various T-gate head sizes. The AlGaN/GaN heterostructure was grown by metal–organic chemical vapor deposition on a 4-in. SiC substrate. The epitaxial layers were composed of a 2 μm-thick Fe-doped GaN buffer, 100 nm-thick GaN channel, and 25 nm-thick $Al_{0.25}Ga_{0.75}N$ barrier. To form the source–drain ohmic contact, Ti/Al/Ni/Au was deposited by an e-beam evaporator followed by rapid thermal annealing at 775°C for 30 s. For device isolation, phosphorus was implanted outside the active area of GaN HEMT. A 60 nm-thick SiN layer was deposited using plasma-enhanced chemical vapor deposition, which acted as the first device passivation layer. The source–drain contact was opened using a buffered oxide

22337326, 2024, 6, Downloaded from https://onlinelibrary.wiley.com/doi/10.4218/etrij.2023-0250 by Electronics and Telecommunications, Wiley Online Library on [06/01/2025]. See the Terms and Conditions (https://onlinelibrary.wiley.com/terms-and-conditions) on Wiley Online Library for rules of use; OA articles are governed by the applicable Creative Commons License

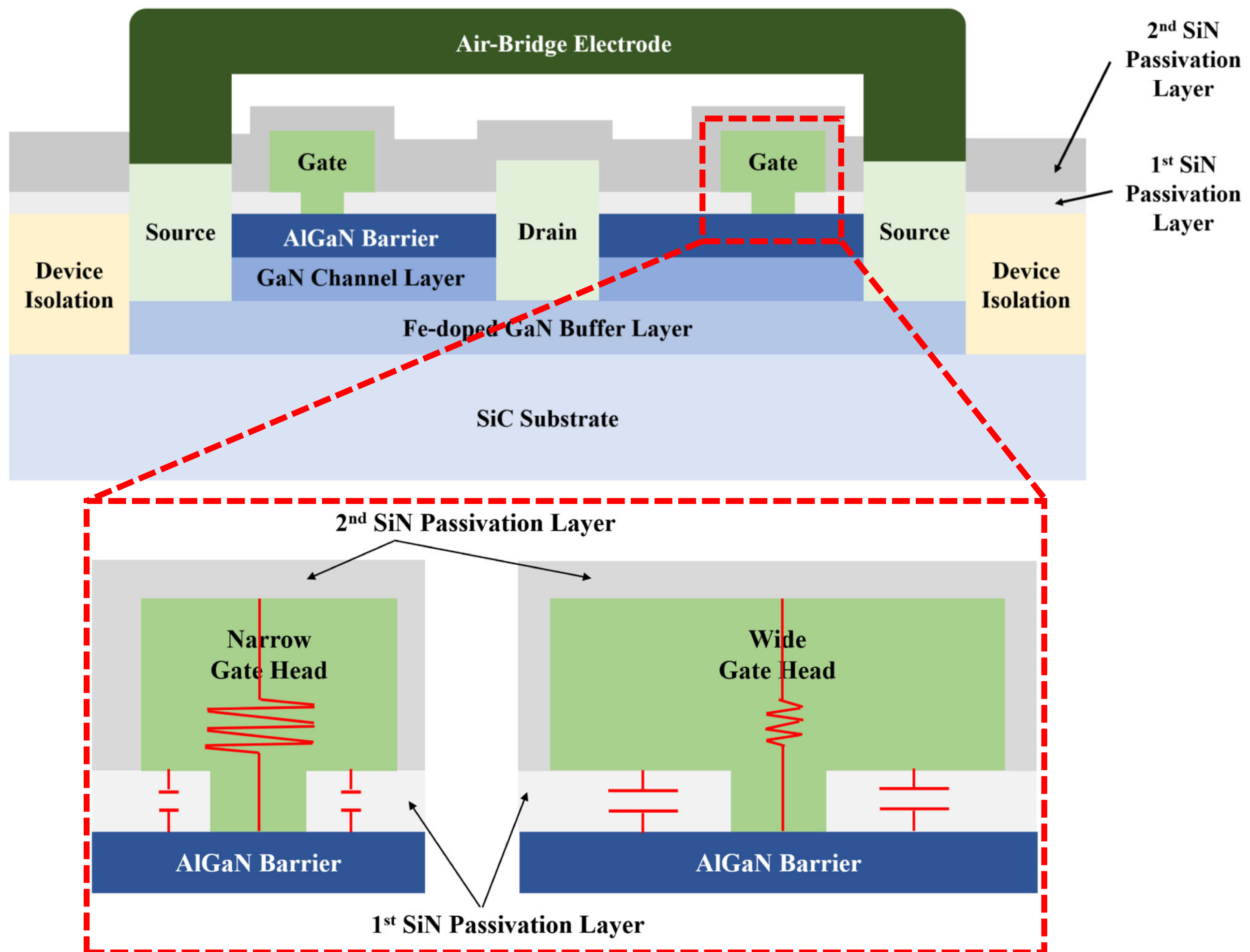

FIGURE 2 Schematic cross-sectional view of GaN HEMT fabricated in this study. The parasitic gate capacitance and gate resistance are conflicting parameters in this structure.

etchant. Ti/Au was deposited using an e-beam evaporator to form the source–drain contact pad. The gate foot (i.e., gate length) was patterned and etched using e-beam lithography and inductively coupled plasma, respectively.

To vary the size of the T-gate head, it was patterned using e-beam lithography. Ni/Au was deposited using an e-beam evaporator to form a T-gate electrode. A 250 nm-thick SiN layer was deposited via plasma-enhanced chemical vapor deposition as the second device passivation layer. To form the contact via, this passivation layer was etched using inductively coupled plasma. The air-bridge electrode was formed by 3 μm-thick Au plating for the connection of the separated source pads.

Scanning electron microscopy images of the fabricated GaN HEMTs and cross-sections of the T-gate electrode prepared in this study are shown in Figure 3. The gate length (L_G), unit gate width (W_G), and number of gate fingers (N_F) were 0.15 μm, 100 μm, and 2, respectively. The distances between the source and drain (L_{SD}), source and gate (L_{SG}), and gate and drain (L_{GD}) were 5.0, 1.125, and 3.725 μm, respectively. The T-gate head size was varied from 0.83 to 1.08 μm.

The DC (transfer and output characteristics) and RF (f_T and f_{max}) performances were measured to investigate and compare the device characteristics according to the T-gate head size. On-wafer measurements were performed using a probe station with ground–signal–ground probe contacts. For the transfer characteristics measurements, the drain current (I_D) was measured at drain bias (i.e., applied voltage at drain electrode) $V_D = 10$ V, while gate bias (i.e., applied voltage at gate electrode) V_G was swept from −6.0 to 0.0 V.

22337326, 2024, 6, Downloaded from https://onlinelibrary.wiley.com/doi/10.4218/etrij.2023-0250 by Electronics and Telecommunications, Wiley Online Library on [06/01/2025]. See the Terms and Conditions (https://onlinelibrary.wiley.com/terms-and-conditions) on Wiley Online Library for rules of use; OA articles are governed by the applicable Creative Commons License

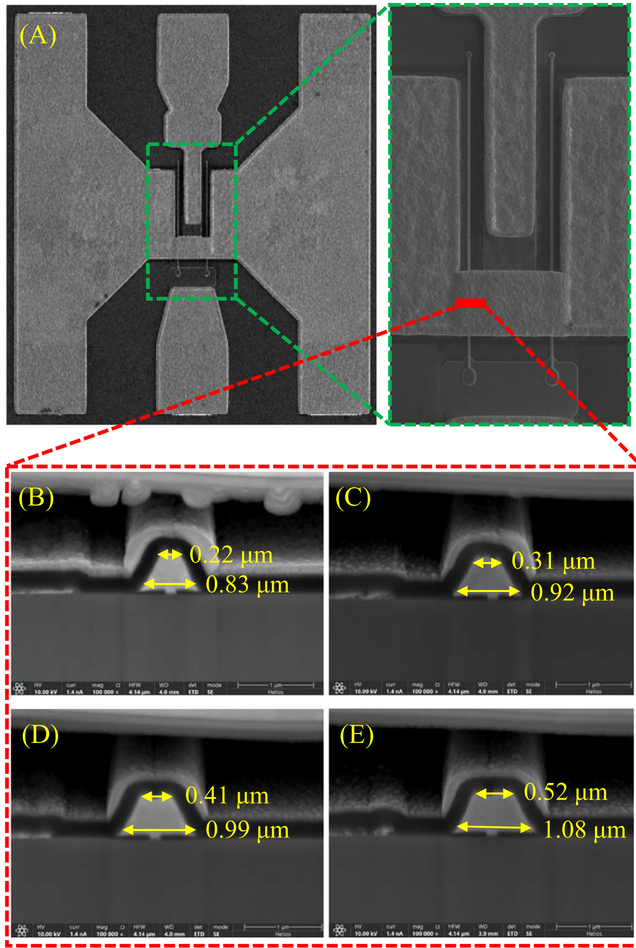

FIGURE 3 Fabricated GaN HEMT and T-gate electrode cross-section. (A) Scanning electron microscope images of fabricated GaN HEMT and magnified view of the T-gate electrode region. Cross-section views of T-gate electrode with head sizes of (B) 0.83 μm, (C) 0.92 μm, (D) 0.99 μm, and (E) 1.08 μm.

The transconductance was obtained from I_D. When the output characteristics were measured, V_G was fixed to 0.0 V and V_D was swept from 0.0 to 20.0 V. To determine the RF performance, we measured the *S*-parameters. To extract f_T, the measured *S*-parameters were converted into *H*-parameters. Then, we fit a line with a −20 dB slope on the H_{21} curve. f_T was defined as the point of the linear line extrapolated to 0 dB. To extract f_{max}, the measured *S*-parameters were converted into the maximum stable gain divided by the maximum available gain. A line with a −20 dB slope was fit at stability factor $K = 1$. The extrapolated point of the line at 0 dB was determined to be f_{max}.

3 | RESULTS AND DISCUSSION

3.1 | DC characteristics

To investigate the DC characteristics, we measured the typical device transfer and output characteristics of GaN HEMTs with various T-gate head sizes, as shown in Figure 4. As shown in Figure 4A, the GaN HEMTs show an excellent pinch-off property at low gate bias ($V_G < -4$ V). The drain current (I_D) increases with the gate bias (V_G) and exceeds 900 mA/mm at $V_G = 0$ V. The I_D curves overlap in the subthreshold regime (Figure 4B). The conventional bell-shaped transconductance (g_m) behavior is shown in Figure 4C. Figure 4D shows the device output characteristics, where I_D increases as the drain bias (V_D) increases. After reaching maximum I_D at $V_D \approx 10$ V, I_D slightly reduces owing to self-heating [25–27].

The device parameters in terms of the threshold voltage (V_{TH}), maximum g_m ($g_{m,max}$), I_D at $V_G = V_G@g_{m,max} + 2$ V, and subthreshold swing were extracted to precisely evaluate the DC characteristics, which correspond to the T-gate head size in the GaN HEMTs (Figure 5). When the T-gate head size varies from 0.83 to 1.08 μm, no considerable difference in the DC device parameters occur, as shown in Figure 5A,B, D. In Figure 5C, I_D at $V_G = V_G@g_{m,max} + 2$ V decreases with increasing T-gate head size. However, I_D reduces by only 3%. Thus, the difference in the DC characteristics with respect to the T-gate head size is negligible.

3.2 | RF characteristics

To evaluate the RF performance, the *S*-parameters were measured, and f_T and f_{max} were extracted for GaN HEMTs with various T-gate head sizes, as shown in Figure 6. Both f_T and f_{max} were extracted around the $g_{m,max}$ condition (at $V_G = -2.6$ V and $V_D = 10$ V) because the maximum f_T and f_{max} were achieved at this bias condition. As shown in Figure 6C, the RF performance depends on the T-gate head size. When the T-gate head size reduces from 1.08 to 0.83 μm, f_T and f_{max} improve by 27% (from 30.1 to 38.03 GHz) and 26% (from 58.06 to 73.03 GHz), respectively. Therefore, unlike the DC characteristics, the RF performance strongly depends on the T-gate head size. Thus, the opposite effect to that reported in [9–12] is observed. When the T-gate head size increases to reduce gate

22337326, 2024, 6, Downloaded from https://onlinelibrary.wiley.com/doi/10.4218/etrij.2023-0250 by Electronics and Telecommunications, Wiley Online Library on [06/01/2025]. See the Terms and Conditions (https://onlinelibrary.wiley.com/terms-and-conditions) on Wiley Online Library for rules of use; OA articles are governed by the applicable Creative Commons License

resistance R_g, the RF performance of the GaN HEMTs degrades.

3.3 | Small-signal modeling

We performed small-signal modeling to characterize the dependence of the RF performance of GaN HEMTs on the T-gate structure. We extracted the parasitic gate capacitance in terms of C_{gs}, C_{gd}, and R_g because they varied with the T-gate structure and determined f_T and f_{max}.

Parameter extraction was conducted using the method suggested by Berroth and Bosch [28] using S-parameter measurements. Extrinsic elements were considered using the measurement results obtained from the open and short patterns corresponding to the fabricated GaN HEMTs. The measured S-parameters were converted into Y-parameters. The Y-parameters that describe various components are given by

$$Y_{11i} = g_{fs} + f_{fd} + \frac{\omega^2 R_i C_{gs}^2}{1+\omega^2 C_{gs}^2 R_i^2} + \frac{\omega^2 R_{gd} C_{gd}^2}{1+\omega^2 C_{gd}^2 R_{gd}^2} + j\omega\left(\frac{C_{gs}}{1+\omega^2 C_{gs}^2 R_i^2} + \frac{C_{gd}}{1+\omega^2 C_{gd}^2 R_{gd}^2}\right), \quad (3)$$

$$Y_{12i} = -g_{fd} - \frac{\omega^2 R_{gd} C_{gd}^2}{1+\omega^2 C_{gd}^2 R_{gd}^2} - j\omega \frac{C_{gd}}{1+\omega^2 C_{gd}^2 R_{gd}^2}, \quad (4)$$

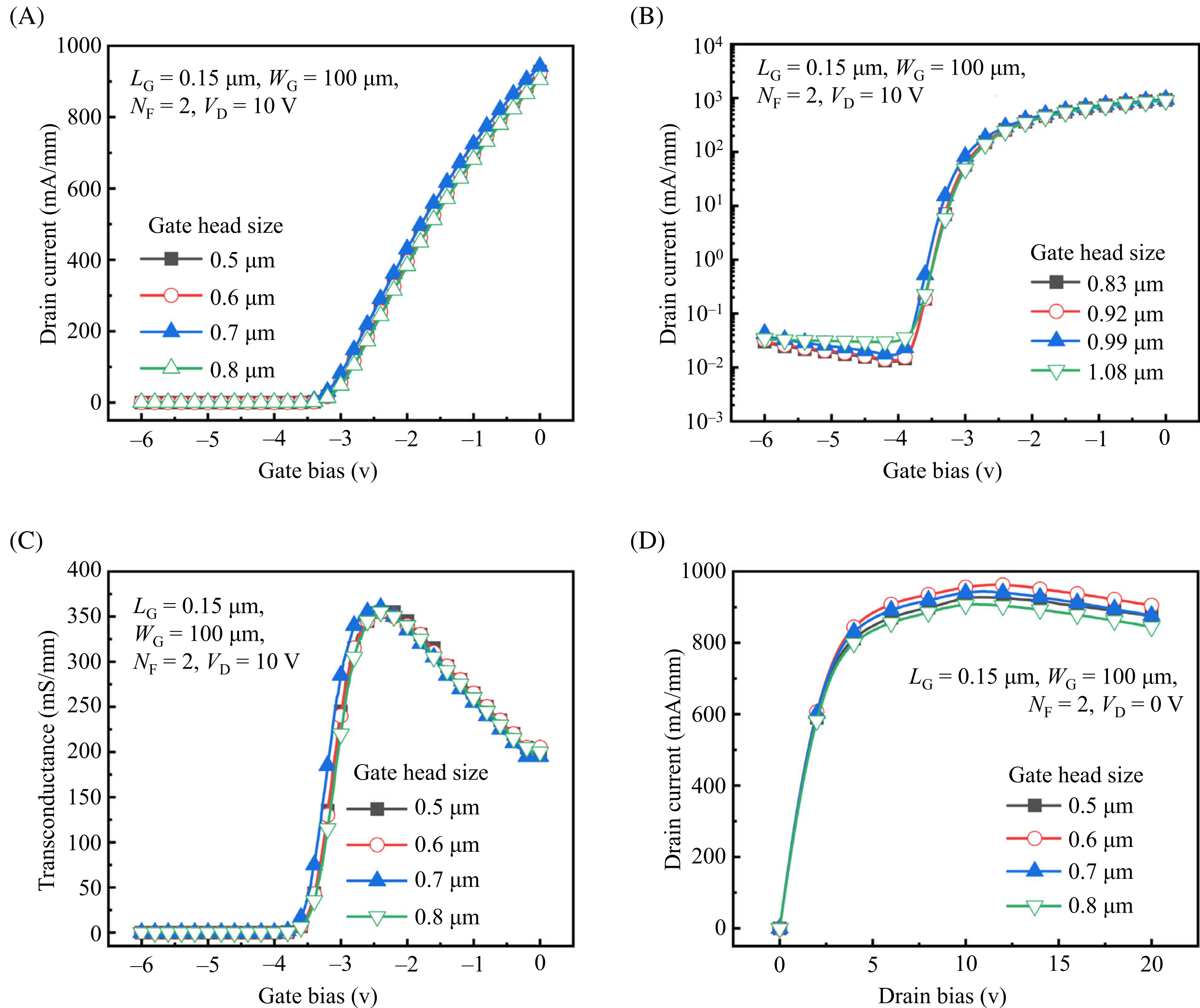

FIGURE 4 Typical transfer and output characteristics of GaN HEMTs with various T-gate head sizes. (A) Drain current (linear scale), (B) drain current (log scale), and (C) transconductance according to gate bias for $V_D = 10$ V. (D) Drain current according to drain bias at $V_G = 0$ V.

22337326, 2024, 6, Downloaded from https://onlinelibrary.wiley.com/doi/10.4218/etrij.2023-0250 by Electronics and Telecommunications, Wiley Online Library on [06/01/2025]. See the Terms and Conditions (https://onlinelibrary.wiley.com/terms-and-conditions) on Wiley Online Library for rules of use; OA articles are governed by the applicable Creative Commons License

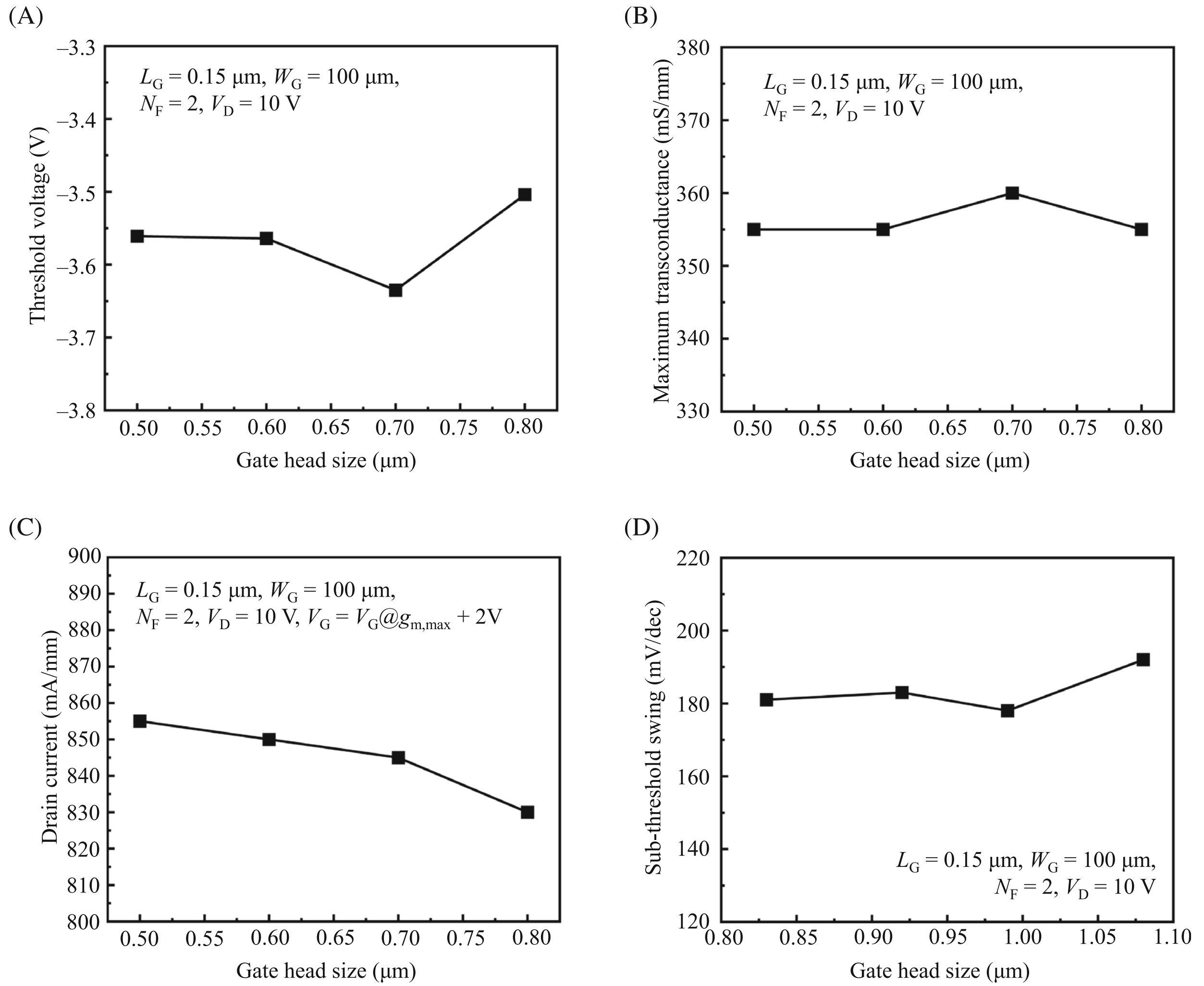

FIGURE 5 DC device parameters in GaN HEMTs for various T-gate head sizes. (A) Threshold voltage, (B) maximum transconductance, (C) drain current at $V_G = V_G@g_{m,max} + 2$ V, and (D) subthreshold swing according to T-gate head size.

$$Y_{21i} = -g_{fd} + \frac{g_m e^{-j\omega\tau}}{1 + j\omega R_i C_{gs}} - j\frac{\omega C_{gd}}{1 + j\omega R_{gd} C_{gd}}, \quad (5)$$

$$Y_{22i} = g_{fd} + g_{ds} + \frac{\omega^2 R_{gd} C_{gd}^2}{1 + \omega^2 C_{gd}^2 R_{gd}^2} + j\omega\left(C_{ds} + \frac{C_{gd}}{1 + \omega^2 C_{gd}^2 R_{gd}^2}\right), \quad (6)$$

where the parameters are determined using the small-signal equivalent circuit shown in Figure 1.

The values of the small-signal model parameters related to the T-gate structure, C_{gd}, C_{gs}, and R_g, were extracted as follows [28]:

$$C_{gd} = -\frac{\mathrm{Im}(Y_{12i})}{\omega}\left(1 + \left(\frac{\mathrm{Re}(Y_{12i}) + g_{fd}}{\mathrm{Im}(Y_{12i})}\right)^2\right), \quad (7)$$

$$C_{gs} = \frac{\mathrm{Im}(Y_{11i}) + Im(Y_{12i})}{\omega}\left(1 + \frac{(\mathrm{Re}(Y_{11i}) + Re(Y_{12i}) - g_{fs})^2}{(\mathrm{Im}(Y_{11i}) + Im(Y_{12i}))^2}\right), \quad (8)$$

22337326, 2024, 6, Downloaded from https://onlinelibrary.wiley.com/doi/10.4218/etrij.2023-0250 by Electronics and Telecommunications, Wiley Online Library on [06/01/2025]. See the Terms and Conditions (https://onlinelibrary.wiley.com/terms-and-conditions) on Wiley Online Library for rules of use; OA articles are governed by the applicable Creative Commons License

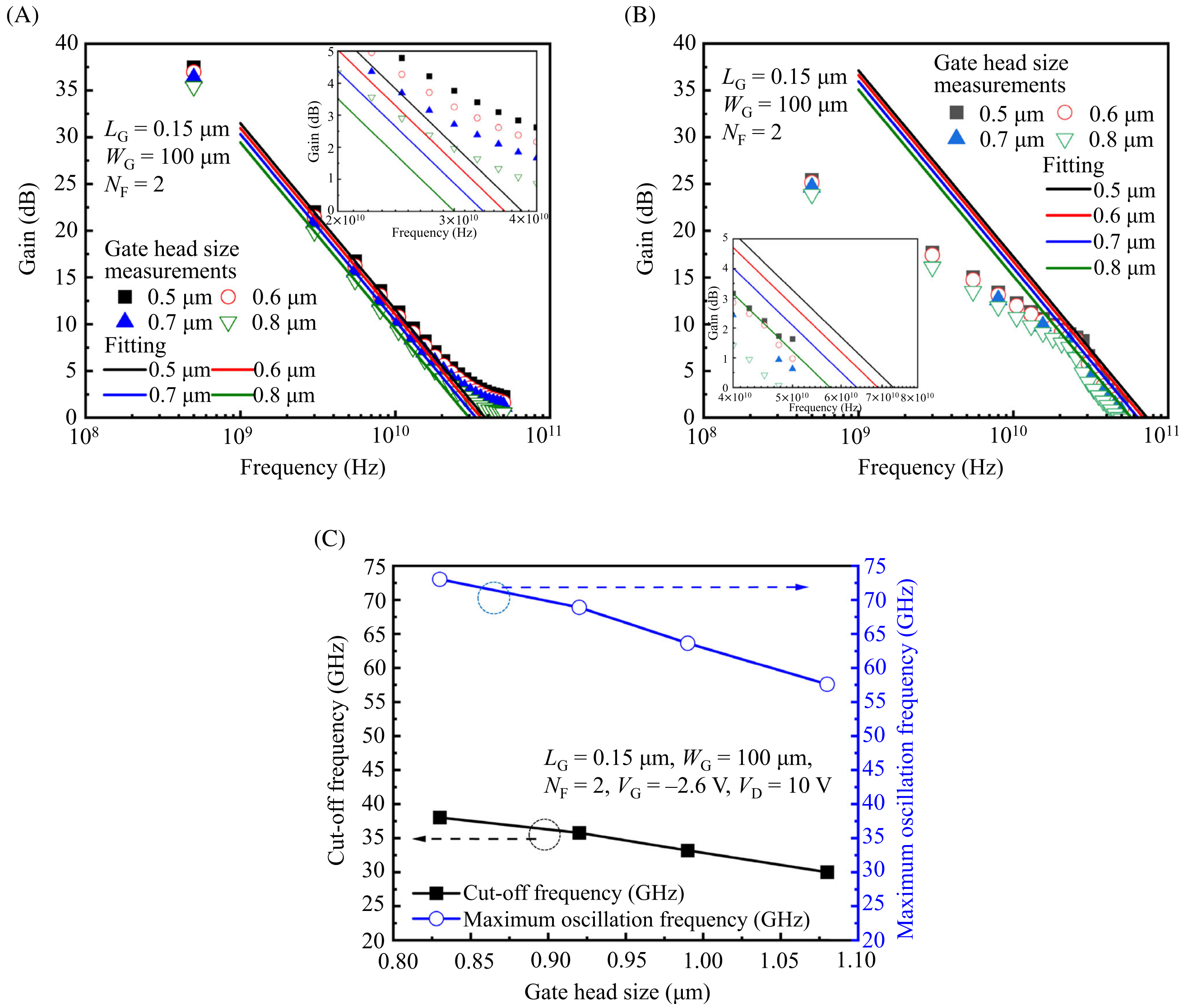

FIGURE 6 RF characteristics in GaN HEMTs for various T-gate head sizes at $V_G = -2.6$ V and $V_D = 10$ V. Gain according to frequency for (A) current-gain cut-off frequency and (B) maximum oscillation frequency. (C) Current-gain cut-off and maximum oscillation frequency according to T-gate head size.

$$\frac{\mathrm{Re}(Y_{11i})}{(\mathrm{Im}(Y_{11i}))^2} = R_g + \frac{\omega^2 C_{gd}^4 R_i R_g}{(C_{gs}+C_{gd})^2} + \frac{C_{gd}^2 R_i}{(C_{gs}+C_{gd})^2}. \quad (9)$$

In Figure 7, C_{gs} and C_{gd} are extracted for GaN HEMTs with various T-gate head sizes because the parasitic gate capacitance depends on the distance between the edges of the gate foot and head. C_{gs} and C_{gd} are extracted at the same bias point, and the maximum f_T and f_{max} values are obtained. When the T-gate head size increases, the distance between the edges of the gate foot and head increases. The area contributing to the parasitic gate capacitance widens. C_{gs} and C_{gd} increase by 19% and 43% at 10 GHz, respectively, under an increasing T-gate head size from 0.83 to 1.08 μm. R_g is also obtained in GaN HEMTs for various T-gate head sizes, as shown in Figure 8. As f_T and f_{max} depend on R_g, R_g varies with the T-gate head size. R_g is extracted at the same bias point as C_{gs} and C_{gd}. When the T-gate head size increases from 0.83 to 1.08 μm, R_g decreases from 1.15 to 0.21 Ω.

22337326, 2024, 6, Downloaded from https://onlinelibrary.wiley.com/doi/10.4218/etrij.2023-0250 by Electronics and Telecommunications, Wiley Online Library on [06/01/2025]. See the Terms and Conditions (https://onlinelibrary.wiley.com/terms-and-conditions) on Wiley Online Library for rules of use; OA articles are governed by the applicable Creative Commons License

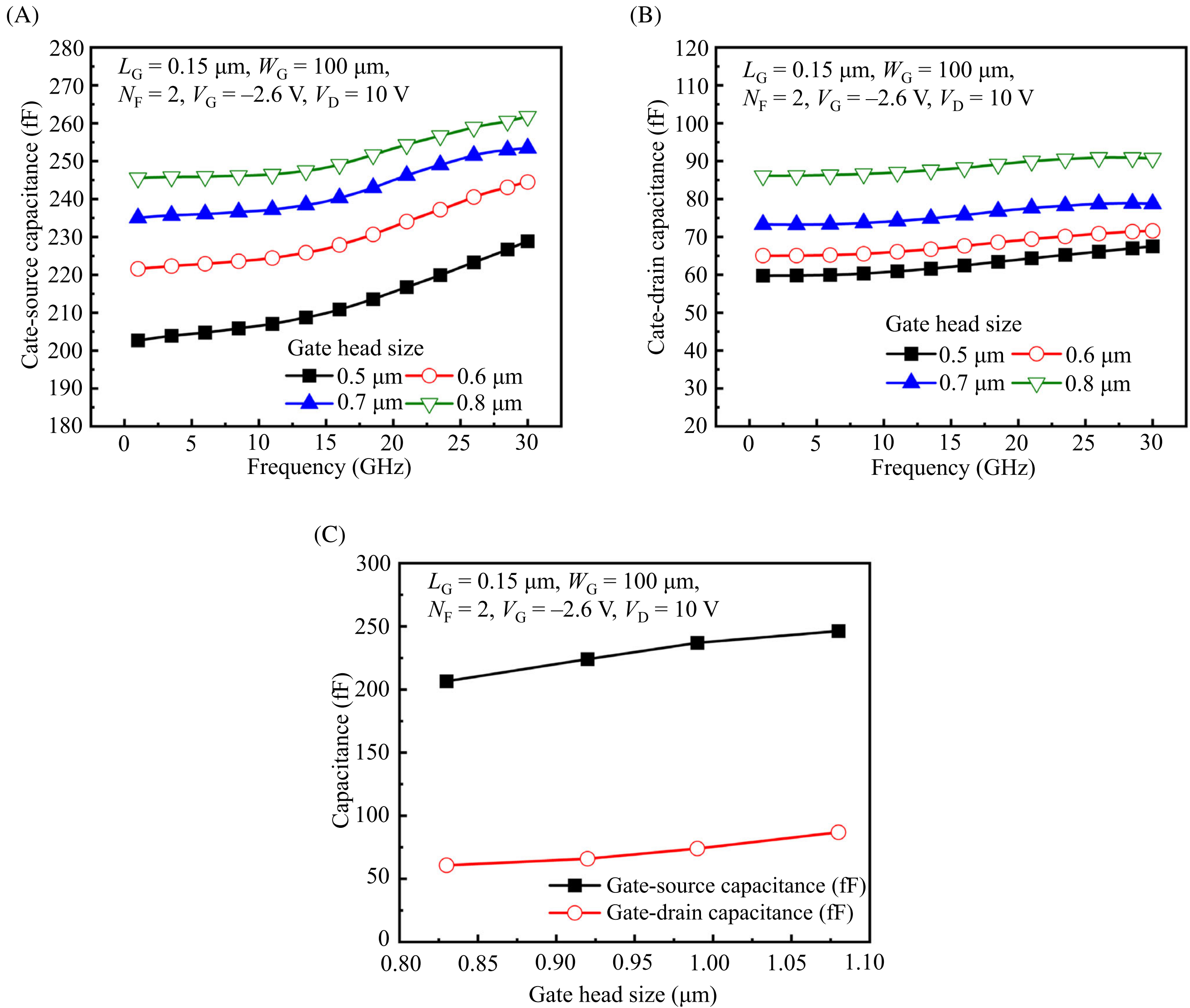

FIGURE 7 Parasitic gate capacitance in GaN HEMTs for various T-gate head sizes. (A) Parasitic gate–source and (B) gate–drain capacitances according to frequency. (C) Parasitic gate–source capacitance and parasitic gate–drain capacitance according to T-gate head size at 10 GHz.

Although R_g reduces by 82%, the RF performance deteriorates when the T-gate head size increases owing to the increased C_{gs} and C_{ds}. Consequently, RF performance parameters, such as f_T and f_{max}, are more sensitive to the parasitic gate capacitance than to R_g . The reduction in the parasitic capacitance is more efficient for improving the RF performance than the reduction in R_g in GaN HEMTs. The device parameters related to the DC and RF properties and parasitic gate capacitance and gate resistance obtained from small-signal modeling are listed in Table 1.

Figure 9 shows the simulated and measured *S*-parameters on a Smith chart to confirm the small-signal modeling results. The simulated and measured *S*-parameters are obtained at $V_G = -2.6$ V and $V_D = 10$ V for frequencies ranging from 1 to 50 GHz. We focus on obtaining precise values near the X-band range. Therefore, a small discrepancy is observed between the simulated and measured *S*-parameters at low frequencies. In the overall frequency range, excellent agreement between the simulated and measured *S*-parameters is observed for GaN HEMTs with various T-gate head sizes, verifying the

22337326, 2024, 6, Downloaded from https://onlinelibrary.wiley.com/doi/10.4218/etrij.2023-0250 by Electronics and Telecommunications, Wiley Online Library on [06/01/2025]. See the Terms and Conditions (https://onlinelibrary.wiley.com/terms-and-conditions) on Wiley Online Library for rules of use; OA articles are governed by the applicable Creative Commons License

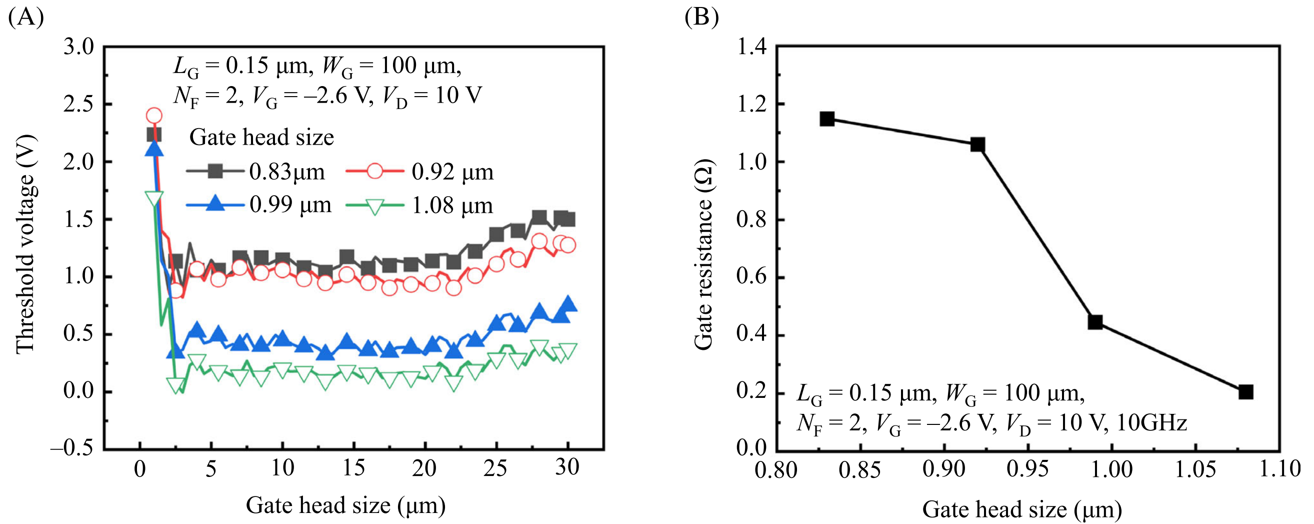

FIGURE 8 Gate resistance in GaN HEMTs for various T-gate head sizes. (A) Gate resistance according to frequency and T-gate head size. (B) Gate resistance according to T-gate head size at 10 GHz.

TABLE 1 Characteristics of GaN HEMTs considered in this study.

Gate head size (μm)	V_{TH} (V)	$g_{m,max}$ (mS/mm)	I_D for $V_G = V_G@g_{m,max} + 2$ V (mA/mm)	Subthreshold swing (mV/dec)	f_T (GHz)	f_{max} (GHz)	C_{gs} (fF)	C_{gd} (fF)	R_g (Ω)
0.83	−3.56	355	855	181	38.03	73.03	206.55	60.66	1.15
0.92	−3.56	354	850	183	35.78	68.91	225.04	65.84	1.06
0.99	−3.64	360	845	178	33.18	63.64	236.91	73.96	0.45
1.08	−3.50	356	830	192	30.01	57.6	246.29	86.86	0.26

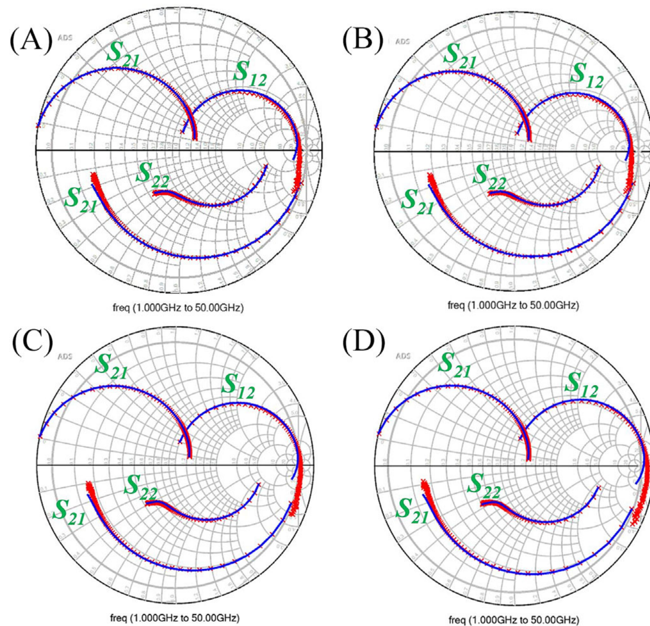

FIGURE 9 Simulated (blue) and measured (red) S-parameters on smith chart for $V_G = -2.6$ V, $V_D = 10$ V, and frequencies ranging from 1 GHz to 50 GHz in GaN HEMTs with T-gate head sizes of (A) 0.83 μm, (B) 0.92 μm, (C) 0.99 μm, and (D) 1.08 μm.

small-signal modeling results and parameter extraction related to the T-gate head size.

4 | CONCLUSIONS

The impact of the T-gate structure, especially head size, on the performance of GaN HEMTs was investigated. The dependence between the T-gate head size and DC characteristics is negligible, but the RF performance strongly depends on the T-gate head size. When the T-gate head size is reduced from 1.08 to 0.83 μm, f_T and f_{max} increase by 27% and 26%, respectively. Small-signal modeling reveals that C_{gs} and C_{gd} decrease by 19% and 43%, respectively, whereas R_g increases by 82% with a reduction in the T-gate head size. Hence, unlike the findings in [9–12], RF performance parameters such as f_T and f_{max} are much more sensitive to the parasitic gate capacitance than to the gate resistance in the proposed HEMT design and fabrication. To improve the RF performance of GaN HEMTs, the minimization of the parasitic gate capacitance by reducing the T-gate head size is more beneficial than reducing the gate resistance.

22337326, 2024, 6, Downloaded from https://onlinelibrary.wiley.com/doi/10.4218/etrij.2023-0250 by Electronics and Telecommunications, Wiley Online Library on [06/01/2025]. See the Terms and Conditions (https://onlinelibrary.wiley.com/terms-and-conditions) on Wiley Online Library for rules of use; OA articles are governed by the applicable Creative Commons License

CONFLICT OF INTEREST STATEMENT

The authors declare that there are no conflicts of interest.

ORCID

Sung-Jae Chang https://orcid.org/0000-0002-6973-8199

REFERENCES

1. J. Kim and Y. Kwon, *High performance millimeter-wave image reject low noise amplifier using inter-stage tunable resonators*, ETRI j. **36** (2014), 510–513.
2. J. Ajayan, D. Nirmal, P. Mohankumar, D. Kuriyan, A. A. Fletcher, L. Arivazhagan, and B. S. Kumar, *GaAs metamorphic high electron mobility transistors for future deep space-biomedical-military and communication system applications: a review*, Microelectron. J. **92** (2019), 104604.
3. W.-S. Park, H.-B. Jo, H.-J. Kim, S.-M. Choi, J.-H. Yoo, H.-S. Jeong, S. George, J.-M. Baek, I.-G. Lee, T.-W. Kim, S.-K. Kim, J. Yun, T. Kim, T. Tsutsumi, H. Sugiyama, H. Matsuzaki, J.-H. Lee, and D.-H. Kim, *Sub-50 nm terahertz $In_{0.8}Ga_{0.2}As$ quantum-well high-electron-mobility transistors for 6G applications*, IEEE Trans. Electron. Devices **70** (2023), 2081–2089.
4. K. H. Hamza and D. Nirmal, *A review of GaN HEMT broad-band power amplifiers*, AEU Int. J. Electron. Commun. **116** (2020), 153040.
5. B.-G. Min, J.-M. Lee, H. S. Yoon, W.-J. Chang, J.-Y. Park, D. M. Kang, S.-J. Chang, and H.-W. Jung, *Analysis of issues in gate recess etching in the InAlAs/InGaAs HEMT manufacturing process*, ETRI j. **45** (2023), 171–179.
6. Y. Tang, K. Shinohara, D. Regan, A. Corrion, D. Brown, J. Wong, A. Schmitz, H. Fung, S. Kim, and M. Micovic, *Ultrahigh-speed GaN high-electron-mobility transistors with f_T/f_{max} of 454/444 GHz*, IEEE Electron. Device Lett. **36** (2015), 549–551.
7. T. Palacios, A. Chakraborty, S. Rajan, C. Poblenz, S. Keller, S. P. DenBaars, J. S. Speck, and U. K. Mishra, *High-power AlGaN/GaN HEMTs for Ka-band applications*, IEEE Electron. Device Lett. **26** (2005), 781–783.
8. K. Shinohara, D. C. Regan, Y. Tang, A. L. Corrion, D. F. Brown, J. C. Wong, J. F. Robinson, H. H. Fung, A. Schmitz, T. C. Oh, S. J. Kim, P. S. Chen, R. G. Nagele, A. D. Margomenos, and M. Micovic, *Scaling of GaN HEMTs and Schottky diodes for submillimeter-wave MMIC applications*, IEEE Trans. Electron. Devices **60** (2013), 2982–2996.
9. K. W. Kobayashi and V. Kumar, *A broadband 70-110 GHz E-/W-band LNA using a 90 nm T-gate GaN HEMT technology*, IEEE Microw. Wirel. Compon. Lett. **31** (2021), 885–888.
10. J. R. Kumar, D. Nirmal, J. Ajayan, and S. Tayal, *Investigation on $L_G = 50$ nm tapered T-gated AlGaN/GaN HEMT on silicon wafer with a f_T/f_{max} of 264/312 GHz for beyond 5G (B5G) applications*, Silicon **14** (2022), 11315–11322.
11. D. Dominijanni, E. Giovine, A. Notargiacomo, A. Pantellini, P. Romanini, M. Peroni, and A. Nanni, *Dual step EBL gate fabrication technology for GaN-HEMT wideband applications*, Microelectron. Eng. **88** (2011), 1927–1930.
12. M. Meryleen, T. De, and A. K. Panda, *Nanoscale T-shaped AlGaN/GaN HEMT with improved DC and RF performance*, Int. J. Nanoparticles **11** (2019), 113–129.
13. B. H. Lee, R. H. Kim, B. O. Lim, G. W. Choi, H. J. Kim, I. P. Hong, and J. H. Lee, *High RF performance improvement using surface passivation technique of AlGaN/GaN HEMTs at K-band application*, Electron. Lett. **49** (2013), 1013–1015.
14. K.-Y. Cheng, S.-C. Wu, C.-J. Yu, T.-W. Wang, J.-H. Liao, and M.-C. Wu, *Comparative study on performance of AlGaN/GaN MIS-HEMTs with SiN_x, SiO_x, and SiNO surface passivation*, Solid-State Electron. **170** (2020), 107824, DOI 10.1016/j.sse.2020.107824.
15. S.-J. Chang, H.-W. Jung, J.-W. Do, K. J. Cho, J.-J. Kim, Y. J. Jang, H. S. Yoon, H.-K. Ahn, B.-G. Min, H. Kim, J.-M. Yang, H.-S. Kwon, and J.-W. Lim, *Enhanced carrier transport properties in GaN-based metal-insulator-semiconductor high-electron mobility transistor with SiN/Al_2O_3 bi-layer passivation*, ECS J. Solid State Sci. Technol. **7** (2018), N86–N90.
16. L. Li, K. Nomato, M. Pan, W. Li, A. Hickman, J. Miller, K. Lee, Z. Hu, S. J. Bader, S. M. Lee, J. C. M. Hwang, D. Jena, and H. G. Xing, *GaN HEMTs on Si with regrown contacts and cutoff/maximum oscillation frequencies of 250/204 GHz*, IEEE Electron. Device Lett. **41** (2020), 689–692.
17. H. Çakmak, M. Öztürk, E. Özbay, and B. Imer, *Nonalloyed ohmic contacts in AlGaN/GaN HEMTs with MOCVD regrowth of InGaN for Ka-band applications*, IEEE Trans. Electron. Devices **68** (2021), 1006–1010.
18. P. Murugapandiyan, S. Ravimaran, J. William, and K. M. Sundaram, *Design and analysis of 30 nm T-gate InAlN/GaN HEMT with AlGaN back-barrier for high power microwave applications*, Superlattices Microstruct. **111** (2017), 1050–1057.
19. R. Angamuthu, B. C. Sengodan, M. Anandan, A. Varghese, and B. S. Vakkalakula, *L_G 55 nm T-gate InGaN/GaN channel based high electron mobility transistors for stable transconductance operation*, Int. J. RF Microw. Comput.-Aided Eng. **32** (2022), e23308.
20. C.-W. Tsou, C.-Y. Lin, Y.-W. Lian, and S. S. Hsu, *101 GHz InAlN/GaN HEMTs on silicon with high Johnson's figure-of-merit*, IEEE Trans. Electron. Devices **62** (2015), 2675–2678.
21. J.-S. Moon, B. Grabar, J. Wong, D. Chuong, E. Arkun, D. V. Morales, P. Chen, C. Malek, D. Fanning, N. Venkatesan, and P. Fay, *Power scaling of graded-channel GaN HEMTs with mini-field-plate T-gate and 156 GHz f_T*, IEEE Electron. Device Lett. **42** (2021), 796–799.
22. J. S. Moon, R. Grabar, J. Wong, M. Antcliffe, P. Chen, E. Arkun, I. Khalaf, A. Corrion, J. Chappell, N. Venkatesan, and P. Fay, *High-speed graded-channel AlGaN/GaN EHMTs with power added efficiency >70% at 30 GHz*, Electron. Lett. **56** (2020), 678–680.
23. R. K. Yadav, P. Pathak, and R. M. Mehra, *TCAD simulations and small signal modeling of DMG AlGaN/GaN HFET*, Int. J. Electr. Comput. Eng. **7** (2017), 1839–1849.
24. T. Palacios, Y. Dora, A. Chakraborty, C. Sanabria, S. Keller, S. P. DenBaars, and U. K. Mishra, *Optimization of AlGaN/GaN HEMTs for high frequency operation*, Phys. Status Solidi **203** (2006), 1845–1850.

22337326, 2024, 6, Downloaded from https://onlinelibrary.wiley.com/doi/10.4218/etrij.2023-0250 by Electronics and Telecommunications, Wiley Online Library on [06/01/2025]. See the Terms and Conditions (https://onlinelibrary.wiley.com/terms-and-conditions) on Wiley Online Library for rules of use; OA articles are governed by the applicable Creative Commons License

25. S. Karmalkar and U. K. Mishra, *Enhancement of breakdown voltage in AlGaN/GaN high electron mobility transistors using a field plate*, IEEE Trans. Electron. Devices **48** (2001), 1515–1521.
26. J. Kuzmik, R. Javorka, A. Alam, M. Marso, M. Heuken, and P. Cordos, *Determination of channel temperature in AlGaN/GaN HEMTs grown on sapphire and silicon substrate using DC characterization method*, IEEE Tans. Electron Devices **49** (2002), 1496–1498.
27. S.-J. Chang, K.-J. Cho, S.-Y. Lee, H.-H. Jeong, J.-H. Lee, H.-W. Jung, S.-B. Bae, I.-G. Choi, H. Kim, H.-K. Ahn, and J.-W. Lim, *Substrate effects on the electrical properties in GaN-based high electron mobility transistors*, Crystals **11** (2021), 1414.
28. M. Berroth and R. Bosch, *High-frequency equivalent circuit of GaAs FETs for large-signal applications*, IEEE Trans. Microw. Theory Tech. **39** (1991), 224–229.

AUTHOR BIOGRAPHIES

Sung-Jae Chang received the BS and MS degrees in electrical engineering from the School of Electrical Engineering and Computer Science, Kyungpook National University, Daegu, Republic of Korea, in 2008 and 2010, respectively, and the PhD degree from the National Polytechnic Institute of Grenoble, Grenoble, France, in 2013. From 2014 to 2015, he was a postdoctoral researcher at Yale University, New Haven, CT, USA. Since 2016, he has been working as a senior researcher at the Electronics and Telecommunications Research Institute, Daejeon, Republic of Korea. His current research interests include the development of GaN-based electronic devices and the effects of radiation on those devices.

Hyeon-Seok Jeong received the BS and MS degrees in electronics engineering from the School of Electronics Engineering, Kyungpook National University, Daegu, Republic of Korea. His research involves fabrication, characterization, and modeling of InP high-electron-mobility and heterojunction bipolar transistors.

Hyun-Wook Jung received the BS degree in engineering from the Department of Electronic Engineering, Kyunghee University, Yongin, Republic of Korea, in 2012 and the MS degree in engineering from the Department of Electrical and Computer Engineering, Sungkyunkwan University, Suwon, Republic of Korea, in 2014. He studied a Ge n-channel metal–oxide–semiconductor field-effect transistor for CMOS logic applications. Since 2015, he has worked at the Electronics and Telecommunications Research Institute, Daejeon, Republic of Korea, where he is now a senior researcher. His current research interests include the design, fabrication, and characterization of electronic devices based on compound semiconductors.

Su-Min Choi is a PhD candidate in electronics engineering at the School of Electronics Engineering, Kyungpook National University, Daegu, Republic of Korea. She received the BS and MS degrees in electronics engineering and electrical engineering from Kyungpook National University, Seoul, Republic of Korea, in 2021 and 2022, respectively. Her research involves the characterization and compact modeling of III-V nanoelectronics, including InP and GaN high-electron-mobility transistors as well as multi-bridge-channel field-effect transistors.

Il-Gyu Choi received the BS, MS, and PhD degrees in materials engineering from Jeonbuk National University, Jeonju, Republic of Korea, in 2008, 2014, and 2016, respectively. He is currently a researcher at the Electronics and Telecommunications Research Institute. His research interests include the growth of III-V nanostructures, optoelectronics using III-nitride nanowires, heat dissipation of optoelectronic semiconductors, and fabrication of III-V based electronic devices.

Youn-Sub Noh received the BS degree in electronics engineering from Chunbuk National University, Jeonju, Republic of Korea, in 2000, and the MS and PhD degrees in electrical and electronics engineering from the Korea Advanced Institute of Science and Technology, Daejeon, Republic of Korea, in 2001 and 2004, respectively. Since 2004, he has been the principal engineer at the Electronics and Telecommunications Research Institute. His research interests include the analysis of the nonlinearities of microwave amplifiers, monolithic microwave integrated circuit power amplifiers, and radiofrequency front-end monolithic microwave integrated circuits for radar and communications.

22337326, 2024, 6, Downloaded from https://onlinelibrary.wiley.com/doi/10.4218/etrij.2023-0250 by Electronics and Telecommunications, Wiley Online Library on [06/01/2025]. See the Terms and Conditions (https://onlinelibrary.wiley.com/terms-and-conditions) on Wiley Online Library for rules of use; OA articles are governed by the applicable Creative Commons License

Seong-Il Kim received the BS degree in electrical engineering from Hanyang University, Seoul, Republic of Korea, in 1998, the MS degree in electrical engineering from the Korea Advanced Institute of Science and Technology, Daejeon, Republic of Korea, in 2000, and the PhD degree in electrical engineering from Chungnam University, Daejeon, Republic of Korea, in 2019. Since 2000, he has been with the Electronics and Telecommunications Research Institute, Daejeon, Republic of Korea, as a member of the research staff, where he has been engaged in research on the design of optoelectronic digital integrated circuits and radiofrequency power amplifiers. He is currently the director of the Defense RF Packaging Research Section. His primary research interests include the design of W-band SiGe radiofrequency and GaN monolithic microwave integrated circuits for transceiver modules.

Sang-Heung Lee received the BS, MS, and PhD degrees from the Department of Electronics Engineering, Chungnam National University, Daejeon, Republic of Korea, in 1988, 1992, and 1998, respectively. From April 1998 to June 1999, he was a postdoctoral researcher at the Electronics and Telecommunications Research Institute, and from March 2009 to February 2011, hardware was an adjunct professor at Chungnam National University. He served as a principal researcher at the Electronics and Telecommunications Research Institute since July 1999, acting as the leader of the SiGe Devices and Circuit Team from 2005 to 2008. His research interests include design in the field of radiofrequency integrated circuits, high-speed analog/digital communication circuits, semiconductor device modeling, and SPICE parameter extraction and optimization. He has authored and co-authored 200 papers published in international and domestic journals and conference proceedings. He also holds 93 patents for semiconductor devices and circuits. He is a member of the Institute of Electronics and Information Engineers, Korea Information and Communication Society, and Korean Institute of Electromagnetic Engineering and Science.

Ho-Kyun Ahn received the BS and MS degrees in materials science and engineering from Korea University, Seoul, Republic of Korea, in 1999 and 2001, respectively. In 2001, he joined the Electronics and Telecommunications Research Institute (ETRI) of Korea, where he has been engaged in research on compound semiconductor devices and monolithic microwave integrated circuits. He received the PhD degree in electronics from Kyungpook National University, Daegu, Republic of Korea, in 2016. He is a principal member of the engineering staff in the RF/Power Components Research Section of ETRI. His current research interests include fabrication and characterization of GaN-based devices and monolithic microwave integrated circuits.

Dong Min Kang received the PhD in radiocommunication engineering from Chungbuk National University, Cheongju, Republic of Korea, in 2009. In 2000, he joined the Electronics and Telecommunications Research Institute, Daejeon, Republic of Korea, where he participated in the study of micro/mm-wave monolithic microwave integrated circuit design for wireless communication and radar systems, and he is currently a director of the RF/Power Components Research Section. His research interests include monolithic microwave integrated circuit design, radiofrequency front-end module design, and packaging.

Dae-Hyun Kim received the BS degree in electronics engineering from the School of Electronics Engineering, Kyungpook National University, Daegu, Republic of Korea, in 1998 and the MS and PhD degrees in electrical engineering from Seoul National University, Seoul, Republic of Korea, in 2000 and 2004, respectively. From 2008 to 2015, he worked for the Massachusetts Institute of Technology as a postdoctoral researcher and research scientist. Since 2015, he has been with the Department of Electronics Engineering, Kyungpook National University, Daegu, Republic of Korea, where he is currently a professor. His main research interests include III-V nanoelectronics with high speed and

22337326, 2024, 6, Downloaded from https://onlinelibrary.wiley.com/doi/10.4218/etrij.2023-0250 by Electronics and Telecommunications, Wiley Online Library on [06/01/2025]. See the Terms and Conditions (https://onlinelibrary.wiley.com/terms-and-conditions) on Wiley Online Library for rules of use; OA articles are governed by the applicable Creative Commons License

functionality and their integration into millimeter-wave/THz integrated circuits, including conventional and GaN high-electron-mobility transistors, multi-bridge-channel and tunnel field-effect transistors, and heterojunction bipolar transistors.

Jong-Won Lim received the BS, MS, and PhD degrees in physics from Chung-Ang University, Seoul, Republic of Korea, in 1988, 1990, and 1998, respectively. In 2000, he joined the Electronics and Telecommunications Research Institute of Korea as a member of the Senior Research Staff, where he has been engaged in research on compound semiconductor monolithic microwave integrated circuit development for radar and wireless telecommunications. His current research interests include the process development, fabrication, and characterization of GaN-based high-electron-mobility transistors and monolithic microwave integrated circuits for millimeter-wave applications.

How to cite this article: S.-J. Chang, H.-S. Jeong, H.-W. Jung, S.-M. Choi, I.-G. Choi, Y.-S. Noh, S.-I. Kim, S.-H. Lee, H.-K. Ahn, D. M. Kang, D.-H. Kim, and J.-W. Lim, *Effects of parasitic gate capacitance and gate resistance on radiofrequency performance in $L_G = 0.15$ µm GaN high-electron-mobility transistors for X-band applications*, ETRI Journal **46** (2024), 1090–1102, DOI 10.4218/etrij.2023-0250.

22337326, 2024, 6, Downloaded from https://onlinelibrary.wiley.com/doi/10.4218/etrij.2023-0250 by Electronics and Telecommunications, Wiley Online Library on [06/01/2025]. See the Terms and Conditions (https://onlinelibrary.wiley.com/terms-and-conditions) on Wiley Online Library for rules of use; OA articles are governed by the applicable Creative Commons License